AFRL-AFOSR-UK-TR-2015-0029

Injection of nucleate-boiling slug flows into a heat exchange chamber in microgravity

Jaume Casademunt

UNIVERSITAT DE BARCELONA
CALLE GRAN VIA DE LES CORTS
CATALANES 585
BARCELONA 08007 SPAIN

EOARD GRANT #FA8655-12-1-2060

Report Date: June 2015

Final Report from 20 March 2012 to 19 March 2015

Air Force Research Laboratory
Air Force Office of Scientific Research
European Office of Aerospace Research and Development
Unit 4515, APO AE 09421-4515

REPORT DOCUMENTATION PAGE

Form Approved OMB No. 0704-0188

1. REPORT DATE *(DD-MM-YYYY)*	2. REPORT TYPE	3. DATES COVERED *(From – To)*
1 June 2015	Final Report	**20 March 2012 – 19 March 2015**

4. TITLE AND SUBTITLE

Injection of nucleate-boiling slug flows into a heat exchange chamber in microgravity

5a. CONTRACT NUMBER

5b. GRANT NUMBER

FA8655-12-1-2060

5c. PROGRAM ELEMENT NUMBER

61102F

6. AUTHOR(S)

Dr. Jaume Casademunt

5d. PROJECT NUMBER

5d. TASK NUMBER

5e. WORK UNIT NUMBER

7. PERFORMING ORGANIZATION NAME(S) AND ADDRESS(ES)

UNIVERSITAT DE BARCELONA
CALLE GRAN VIA DE LES CORTS
CATALANES 585
BARCELONA 08007 SPAIN

8. PERFORMING ORGANIZATION REPORT NUMBER

N/A

9. SPONSORING/MONITORING AGENCY NAME(S) AND ADDRESS(ES)

EOARD
Unit 4515
APO AE 09421-4515

10. SPONSOR/MONITOR'S ACRONYM(S)

AFRL/AFOSR/IOE (EOARD)

11. SPONSOR/MONITOR'S REPORT NUMBER(S)

AFRL-AFOSR-UK-TR-2015-0029

12. DISTRIBUTION/AVAILABILITY STATEMENT

Distribution A: Approved for public release; distribution is unlimited.

13. SUPPLEMENTARY NOTES

14. ABSTRACT

This project has tested and optimized a method to produce controlled boiling through a localized nucleation cavity feeding a capillary crossflow forming regular trains of bubbles. The main objective was to achieve control of bubble size and bubble formation frequency, in order to generate regular slug flows in a capillary tube, and to show that the system performance was robust and independent of gravity. The periodic slug flows created by this method can then be potentially used for applications of heat transfer. The system was tested in a demonstrative setup in the form of a serpentine heat exchange device. This work achieved a full quantitative characterization of the capillary boiling system in a broad range of parameters, identifying the different regimes of operation, and showing that the results are indeed robust and independent of gravity. In addition, the investigators identified an idealized version of the problem to provide novel theoretical insights of fundamental interest, giving rise to exact analytical results that are relevant in the context of scaling and universality in kinetics of phase transitions.

15. SUBJECT TERMS

EOARD, micro gravity, nucleate boiling, sluf flow, thermal control

16. SECURITY CLASSIFICATION OF:			17. LIMITATION OF ABSTRACT	18, NUMBER OF PAGES	19a. NAME OF RESPONSIBLE PERSON
a. REPORT	b. ABSTRACT	c. THIS PAGE			Kevin Bollino
UNCLAS	UNCLAS	UNCLAS	SAR	29	19b. TELEPHONE NUMBER *(Include area code)* +44 (0)1895 616163

EUROPEAN OFFICE OF AEROSPACE RESEARCH & DEVELOPMENT (EOARD)

Air Force Office of Scientific Research (AFOSR)

FINAL REPORT

EOARD Grant : FA8655-12-1-2060

PERIOD: 20 March 2012 – 19 March 2015

PROJECT TITLE: Injection of nucleate-boiling slug flows into a heat exchange chamber in microgravity

PI: Jaume Casademunt

HOST INSTITUTION: University of Barcelona

March 2015

CONTENTS

1 ABSTRACT

In this project we have designed, tested and optimized a method to produce controlled boiling through a localized nucleation cavity feeding a capillary crossflow forming regular trains of bubbles. The main objective was to achieve control of bubble size and bubble formation frequency, in order to generate regular slug flows in a capillary tube, and to show that the system performance was robust and independent of gravity. The periodic slug flows created by this method can then be potentially used for applications of heat transfer. We have also tested our system in a demonstrative setup for this purpose in the form of a serpentine heat exchange device. In our study we have completed a full quantitative characterization of the capillary boiling system in a broad range of parameters, identifying the different regimes of operation, and showing that the results are indeed robust and independent of gravity. In addition, inspired on our design we have identified an idealized version of the problem at hand that has provided novel theoretical insights of fundamental interest, giving rise to exact analytical results that are relevant in the context of scaling and universality in kinetics of phase transitions.

2 DESCRIPTION OF RESEARCH TASKS

2.1 DROP TOWER CAMPAIGNS

The research tasks combine several short-term stays at the ZARM Drop Tower facility of ESA in Bremen (Germany) for ground preparation and data acquisition in drop tower experiments, with the design, data processing and analysis, theoretical modelling and interpretation of results performed in Barcelona. The team has performed 5 Drop Tower campaigns with a total of 59 4.7-second Drops and 5 9.4-second launches through the catapult system. The use of the Drop Tower facility was funded by ESA, at an approximate cost of 5000 € per drop. The amount of high quality microgravity time used totals 325 seconds. In addition, two stays at the ZARM facilities have been used for the necessary ground tests and optimization of the experimental setup, thus resulting in a total of 7 research stays in Bremen. Typically, a regular Drop Tower Campaign consisted of two weeks, one for preparation of the drop capsule, and one for the performance of the drops, typically two per day.

PERIOD	TASK DESCRIPTION	DROPS
Dec 10 – Dec 21 (2012)	Ground tests. Proof-of-principle	0
Jan 28 – Feb 16 (2013)	First Drop Tower Campaign	16
Aug 12 – Aug 24 (2013)	Ground tests. Setup optimization	0
Oct 14 – Nov 02 (2013)	Second Drop Tower Campaign	14
Jan 13 – Feb 01 (2014)	Third Drop Tower Campaign	14
July 21 – Aug 02 (2014)	Fourth Drop (+Catapult) Tower Campaign	10 (5+5)
Nov 10 – Nov 22 (2014)	Fifth Drop Tower Campaign	10

2.2 FIRST YEAR: PROOF-OF-PRINCIPLE

The aim of our project was to design and test a gravity-insensitive method to achieve controlled nucleate boiling in microgravity, in order to create regular vapour-liquid slug flows for potential applications in space technology. During the first year of the project we achieved the proof-of-concept status of our proposal, with a successful first campaign of drop tower experiments and the first collection of data.

Design of setup:

The first few months were dedicated to analyze in detail the different alternatives for the design of the first stage of the experimental setup. This was done in close collaboration with the engineers of the ZARM Drop Tower. We came up with a choice of materials and detailed dimensions of all the parts, including the design of the three thermal baths used, and the pressure control system.

Construction and preparation:

The construction of all parts and the acquisition of small instruments for measurement and control (flow meters, pumps, temperature probes, manometers, etc) and materials (tubes, joints, etc) were assumed by the ZARM team.

Simultaneously, our team in Barcelona, with the incorporation of the new postdoctoral researcher funded by the project, continued the theoretical analysis of the problem, in order to anticipate the most critical points of the designed system and the possible solutions and alternatives in case of unsatisfactory performance. At the same time we started preparing the software tools for the image processing and for the numerical simulation of some of the partial aspects of the problem.

Integration and ground tests of the system:

The first part of the assembly and integration of the system was carried out in close collaboration with the ZARM team. Our postdoctoral researcher moved to Bremen for two weeks in December 2012 and took care of the final integration and fine adjustment of the experimental setup. He then carried out the first series of tests of the system in normal gravity.

Design of the first drop campaign.

After acquiring experience with the functioning of the setup, in particular in view of avoiding spurious bubble nucleation at some locations of the test section, and minimizing transient effects, we were in the conditions to design the fist drop campaign, several moths ahead of time. This was done during January 2013.

Realization of the first drop campaign.

We conducted 16 drops at the ZARM Drop Tower in February. We varied different parameters such as pressure and flow rate, in order to have a first collection of data as broad as possible. It was particularly useful to try different dimensions of the nucleation cavity in order to characterize its the performance in different circumstances.

First assessment of drop campaign.

During the last months of the first period of the project we conducted a first visual inspection of all movies from the microgravity experiments, with focus both on the behaviour of the nucleation site and on the evolution of the slug flow downstream, and we started the image processing required for quantitative data analysis.

2.3 SECOND YEAR: OPTIMIZATION

As already mentioned, in the first year of the project we achieved the proof-of-concept status of our proposal, with a successful first campaign of drop tower experiments and the first collection of data. Detailed analysis of these data also brought evidence that there was room for improvement of the setup design in three main aspects: (i) to modify the geometry in such a way that the nucleation cavity is oriented horizontally when on ground, for a better comparison between cases 1g and 0g; (ii) to avoid the sporadic presence of spurious nucleation of bubbles at points of the setup other than the nucleation site; (iii) to avoid the existence of a relatively long transient originated at the sudden change of hydrostatic pressure due to the instantaneous release of the experimental capsule in the drop tower experiments.

Design with a horizontal nucleation cavity:

This point was not required for the proper performance of the system in microgravity, but it was important in order to minimize the effect of buoyancy when the system operated at normal gravity. In this sense, the physics inside the nucleation cavity was less sensitive to gravity, and the comparison of the two cases was

clearer. The solution that was found, in combination with the other aspects below, involved a complete rearrangement of the pieces and an alternative 3D geometry of the pyramidal shape of the nucleation cavity. The new cavity corresponded to one half of the original cavity.

Elimination of spurious nucleation:

The nucleation of bubbles in an overheated liquid is a fluctuation-driven process that is very delicate and sensitive to small material defects in the system (heterogeneous nucleation) and to slight pressure variations. Indeed, the existence of imperfect junctures of material pieces is usually a potential source of spurious nucleation. The occurrence of spurious nucleation was sporadic in our first series of experiments but always uncontrolled, and in general could have a negative impact on the quality of the acquired data. Avoiding this uncontrolled phenomenon was a remarkable challenge. We solved the problem with a different way to cut and assemble the pieces of the different materials around the area of nucleation, in such a way that the potentially dangerous junctures were located sufficiently far from the critical area, and in a position of lower temperature in order to minimize the effect. The new design resulted very satisfactory in this respect and spurious nucleation was virtually eliminated.

Suppression of pressure transients and backflow:

The fact that the experiment is necessarily running for some time at 1g before the capsule is released, implies that likely there may be free vapour-liquid surfaces at different places of the setup. Under these conditions, the sudden transition between 1g and 0g may have nontrivial consequences. In particular, the pressure requires a finite time to relax to the new conditions, and this transient may produce undesired effects, including a transient backflow in the system. To address this problem, a different layout of the elements in the setup was considered, and a crucial bypass in the liquid line connections was introduced. The transient effects were dramatically minimized with these modifications. In addition we included the appropriate pressure sensors at the critical points to check that the transient was virtually eliminated, and to allow the detection of potential additional problems in the functioning of the system.

On-ground tests of different shapes, sizes and materials for the nucleation site:

In addition to all the tests at 1g and 0g associated to the modifications of the original setup, we explored systematically the performance of the nucleation cavity for different shapes, varying the angle and depth of the V-shape. We also considered cavities with rounded boundaries (U-Shaped). Finally we considered different locations of the juncture between the metallic wall and the plastic wall of the cavity. Each of these tests implied the construction of new pieces and in some cases the change manufacturing method fabrication at the ZARM workshop.

Exploration of alternative methods:

In the context of trying to avoid spurious nucleation, the most critical aspect of the setup, we also found interesting to tentatively explore the nucleation of bubbles based on different principles. In particular, we spent some efforts in developing a prototype that induced the bubble formation by exploiting the Venturi effect, through a narrowing of the tube. The prototype system turned out to perform unsatisfactorily, mostly due to the induced turbulence of the flow. This caused the bubbles to break up into very small and irregular sizes. In other, parameter regimes, the system created a very elongated bubble. The inherent instability of the flow configuration prevented us to reasonably achieve the intermediate regime of bubble sizes between these two extreme regimes. We finally abandoned this idea at the point that the spurious nucleation problem was solved with the different strategy explained above.

2.4 THIRD YEAR: CHARACTERIZATION, MODELLING AND APPLICATION

The third year was devoted to the systematic characterization and calibration of the final design of the device with the nominal two types of nucleation cavity (conductive and isolating), with focus on demonstrating the insensitivity to gravity of its performance. We completed the series of the necessary drops to explore parameter space, and completed the data analysis. As a simple application of our system, we also designed, constructed and tested a heat exchange device in the form of a serpentine tube where the created slug flows were injected. This was tested in 0g and 1g, and the heat exchange was measured for different parameters. Finally we developed a theoretical model to discuss some implications of our study in fundamental physics. At the time of writing this report, two papers are in preparation to publish the results obtained.

Heat exchange device:

The main novelty of the experimental setup in this third period was the assembly a new heat exchange device at the end of the line. This substituted the original heat exchange chamber originally planned in the proposal. The idea was to illustrate the application of the regular slug flows produced by our system, in a system that could provide higher quality data of heat exchange as compared to the illustrative purposes of the orginal proposal, involving a larger chamber for which the temperature control would be more difficult, and where residual flows of the preparation stage of the experiment would also complicate the analysis. We designed a piece of metal with resistors and thermal sensors, with a transparent serpentine tube that conducted the injected slug flow. As the slug flow advances, the bubbles increase or decrease size depending on the temperature of the metal. From the bubble sizes one can infer the heat transfer between the slug flow and its environment. The heat losses of the system to the environment could be measured for different temperature by generating steady situations without liquid flow, with control of the dissipated heat at the resistors. This system was ready for both ground and microgravity tests in the campaign of July 2014. Once proven the independence of gravity of its behaviour, in the last campaign of November 2014 the systematic measurements of heat exchange were carried out on ground.

Catapult system:

In the campaign of July 2014, we also tried an adaptation of our experimental system to the catapult launch system. This possibility was not foreseen in our original plan, but was offered by the ZARM technical team at no extra cost. This mode of operation of the ZARM Tower doubles the total microgravity time to 9.4 seconds, but involves an initial phase with strong acceleration for the launch from the ground level. This produces a sequence of variable hyper-gravity prior to microgravity, which may introduce additional transients depending of the initial setup configuration. We agreed to try with the idea of testing whether the transients could decay fast enough to eventually yield a period of valid data longer than with ordinary 4.7 s drops. After 5 trials we finally concluded that this was not the case and decided to go back to the original drop protocol for the rest of the experiments in that and the subsequent campaign.

Complete exploration of parameter space in 1g and 0g:

The specifications of the drops for the two last campaigns aimed at having a complete phase diagram of operation of the final setup with both conducting and isolating nucleation cavities. The performance of the system was calibrated for a broad range of two main parameters: cross-flow injection rate and effective pressure at the nucleation cavity. The different operation modes defined for the system in the previous period were delimited in the above diagram. The same diagram was completed for both 0g and 1g to prove the insensitivity of the system to gravity.

Bubble frequency and heat transfer at the nucleation site:

The pressure-flow phase diagrams above were extended with the measurement of an additional independent variable that is relevant for possible applications, namely the bubble formation frequency. This was obtained for the different modes of operation of the two nominal nucleation cavities (conducting and isolating), for both 1g and 0g. One of the interesting properties of our nucleation system that was highlighted already at early stages of the project, is that the size of bubbles at the exit of the cavity is expected to be essentially independent of parameters, and determined basically by the geometry of the cavity. This observation, however, is only approximate, and some significant deviations from this behaviour were found in some parameter regimes. To characterize this feature, we directly measured systematically the average bubble size for all parameter values at the exit of the nucleation site. This quantity combined with the bubble formation frequency allowed us to compute the total rate of liquid-vapor transformation, which yields directly the total heat absorbed per unit time at the cavity.

Theoretical model an exact scaling results:

Finally, in this period we have completed a theoretical study of the conducting nucleation cavity. With some reasonable simplifications, we have been able so show not only the existence of a selfsimilar solution, but we have used this to define a simplified numerical model to account for multiple bubbles including bubble coalescence in the cavity. We have numerically simulated the model and checked the scaling regime. We have also studied this model analytically and proved exactly the exponent of scaling of the problem.

3 SUMMARY OF RESULTS

3.1 OVERVIEW

The main novelty and advantage of our design is that it generates bubbles from boiling with a given size that is roughly independent of the liquid crossflow that pulls away the bubbles and of the heat transfer rate and the nucleation site. Once established that the bubble size is essentially fixed by geometry, the heat transfer rate (a difficult parameter to control) is then directly inferred from the frequency of bubble formation, a simple observable that is directly accessible from the image recording. The practical applicability of the device depends on the good control of the number and size of bubbles, but also on their regularity. The aim is thus to achieve that the outlet of the measuring section delivers a uniform and period slug flow of identical bubbles, with parameters that can be well controlled. Taking into account that the nucleation of vapour bubbles is an inherently noisy and delicate phenomenon, since it corresponds to the relaxation of a metastable state (overheated liquid), it is remarkable that a good control of the process can be achieved. In the late stages of the project we have illustrated the use of the slug flows created by our device by injecting them in a serpentine tube for heat exchange, and have measured the heat exchange per unit area and as a function of the temperature difference between a hot contact and the injected slug flow.

During the project we tested a variety of shapes and sizes of the nucleation cavity, and different locations of the juncture between the two materials of the walls of the cavity. We gained experience and identified the optimal design of the cavity that we would use for a systematic characterization and calibration. In Figs.3.1 and 3.2 we show a representative example of the good operation of the nucleation cavity and two examples of the resulting slug flows downstream the measuring section, from the first campaign of February 2013.

We identified two basic configurations of the nucleation cavity, namely the *conductive cavity,* where most of the hot wall (on the left in Fig.3.1) is metallic, except for a small part at the outlet, and the *isolating cavity,* where most of the hot wall is made of plexiglass. In addition, we distinguished two main modes of operation of the nucleation cavities, namely the *single-bubble regime* and the *multiple-bubble regime.* The first one is the most interesting for practical purposes and corresponds to the case in which the cavity is continuously filled by a single bubble that breaks up when exposed to the crossflow. The latter drags the bubbles downstream forming a regular train of bubbles. This mode produces a high frequency of regular bubble formation and resembles the behaviour of the T-juntion previously studied by the group where air and water where mixed (Carrera et al. AIAA J. 46, 2010 (2008)). As discussed below, it is convenient to define also an intermediate regime where there are only two bubbles, with a single slug of liquid advancing through the cavity and ejecting one of the bubbles.

From a theoretical and fundamental point of view it is interesting to study the cases of bubble trains inside the nucleation cavity, in both the conducting and the isolating cavity. With regards to the first one, we already identified, in the first year of the project, a scaling solution in which the bubbles advance at constant velocity and adopt a self-similar growing shape. Furthermore, in the case where there are significant coalescence events inside the cavity, one can adapt the self-similar assumption in a statistical sense. In the case of the isolating cavity, the self-similar solution is not achieved due to the significant temperature gradients along the cavity. It is worth remarking that regardless of the different dynamics of bubbles inside the cavity, in all cases the bubble size at the outlet of the nucleation cavity is relatively constant. A detailed quantitative analysis, however, show that some dependence can be found in some regimes, similarly to the weak dependence of bubble size reported by Carrera et al (2008) in a similar situation, and that will be discussed later.

The overall parameter ranges of operation of the system were delimited. The most sensitive parameter is the pressure at the measuring section. The system has been tested in the range 0.95 – 1.25 bar. Note that changing this pressure effectively modifies the overheating of the incoming liquid without modifying the temperature. Similarly, changes in temperature may be translated to different effective pressures. We usually worked in a range of approximately 5 degrees of the temperature at the Aluminum heater (typically between 61.5º C and 66.5º C). The crossflow volume rate was typically in the range 10 – 60 ml/min. The frequency of bubble injected in the crossflow varied very much, reflecting the different heat transfer conditions. The values of bubble injection frequency range between 20 bubbles/second and 200 bubbles/second.

3.2 FIRST DROP TOWER CAMPAIGN

Figs.3.1 and 3.2 show representative examples of the nucleation cavity in the multiple-bubble regime, for a conducting cavity, and of the slug flows created downstream. Fig.3.3 illustrates the image processing involved in the particle-tracking algorithm, and show the time evolution of bubbles inside the cavity.

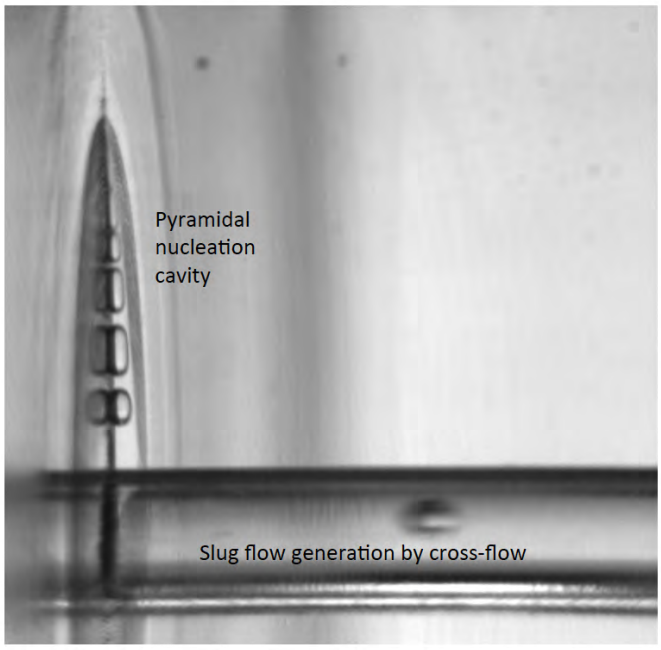

Fig.3.1 View of the pyramidal nucleation cavity where bubbles are formed in contact with the hot wall on the left. The bubbles grow as they absorb heat and move towards the opening of the cavity, where they are dragged by a crossflow (first campaign, February 2013).

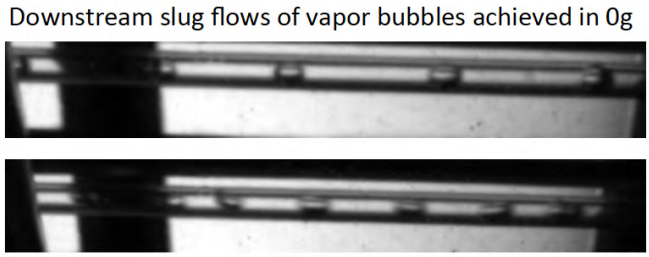

Fig.3.2 View of two representative slug flows far from the nucleation cavity, where bubbles continue to grow due to the overheating of the liquid, but preserve the periodicity of the bubble train (February 2013).

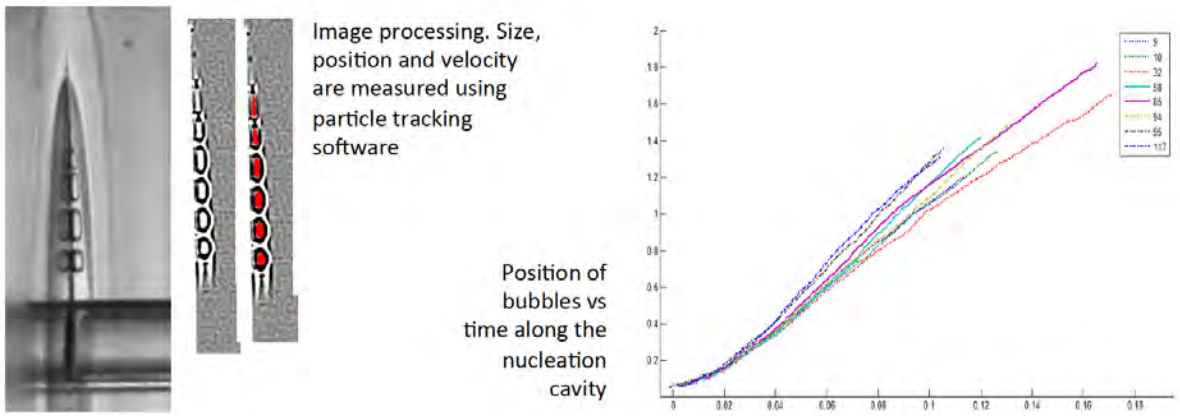

Fig.3.3 On the left, example of the image processing of the nucleation cavity to be used in a particle tracking algorithm. On the right, position of bubbles as a function of time, setting t=0 for each bubble as the initial position in the nucleation cavity. This shows the approximate linear growth, corresponding to a 'conducting cavity' (metallic contact with the heater). Data correspond to the first campaign (February 2013).

Figs 3.4 and 3.5 characterize the slug flow downstream for 0g and 1g, in terms of length, volume and velocity of bubbles. The length is more sensitive to gravity because the positioning of the bubble in the section of the capillary allows for different shapes, different heat transfer conditions and different velocity.

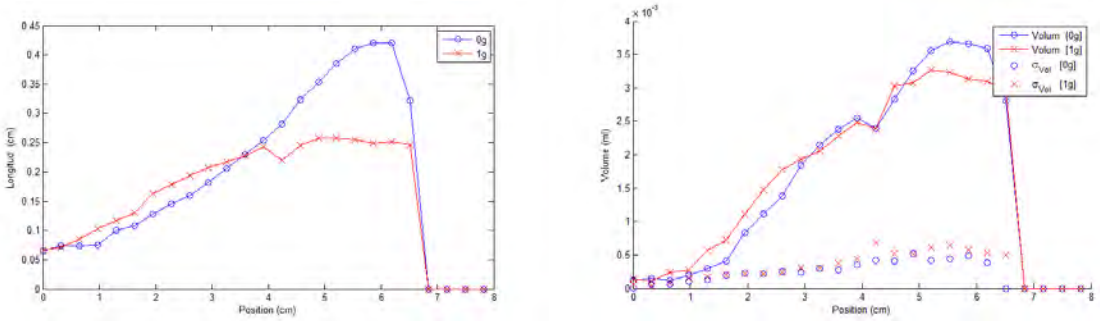

Fig.3.4 Downstream slug flow. Left graphic plots the average length of bubbles at a given position. Right panel plots the average volume of bubbles at a given position, and its standard deviation (data from campaign of February 2013).

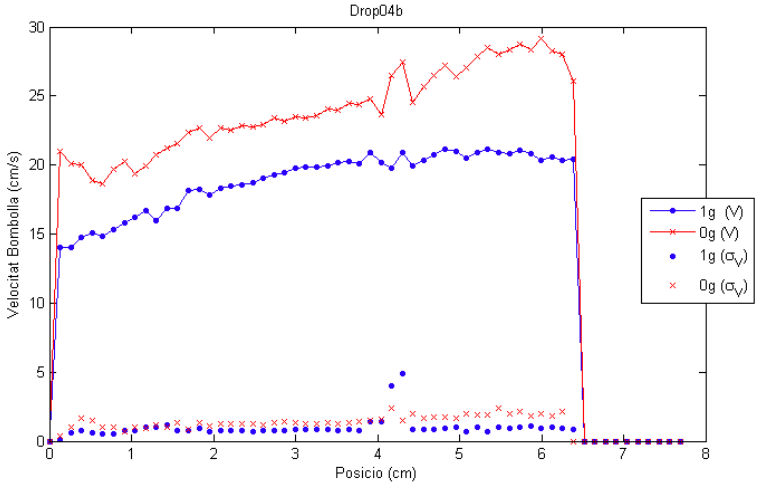

Fig.3.5 Average velocity of bubbles downstream, and standard deviation. Note the systematic difference of bubble speed between 1g and 0g.

3.3 SECOND AND THIRD DROP TOWER CAMPAIGNS

As before, here we only give a representative sample of the data collected and analyzed. As mentioned above, the setup was significantly improved prior to the third campaign. The slug flows generated were significantly more regular and controlled in the new setup. In these campaigns our attention was mostly focussed on the performance of the nucleation cavity. The two main modes of operation are illustrated in Fig. 3.5(a) and (b). A snapshot representative of the intermediate mode is shown in Fig.3.5(c)

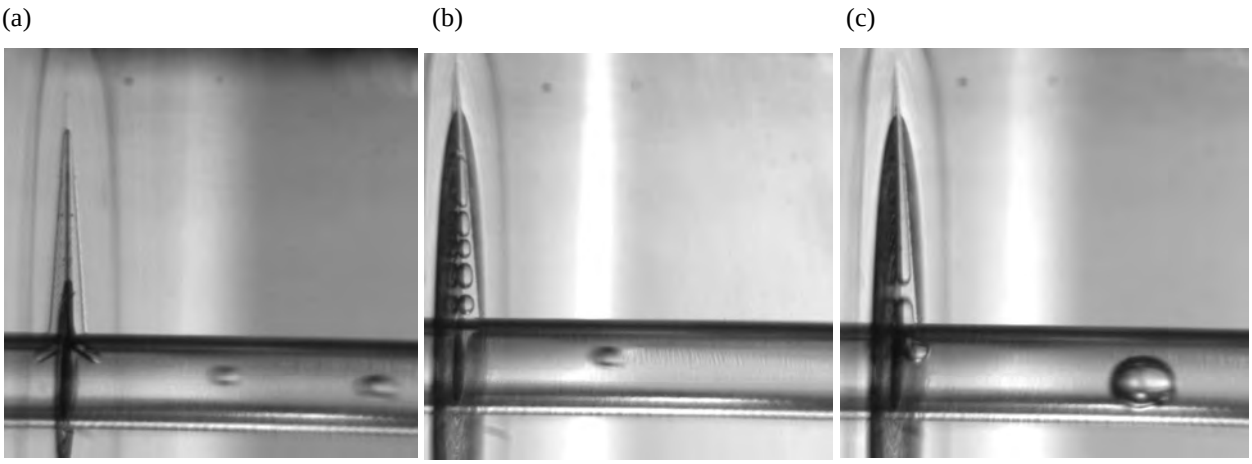

Fig.3.6 Representative snapshots of the main modes of operations of the nucleation cavity: (a) Single-bubble mode; (b) Multi-bubble mode; (c) Intermediate mode, with 1-2 bubbles inside the cavity.

From a fundamental point of view, the most interesting aspect to study is the physics of bubble growth and interaction in the multi-bubble regime, both in the presence and absence of coalescence, and comparing the conditions of conductive or isolating contact with the heater. Some representative measurements obtained from the particle-tracking techniques developed are shown for instance in Fig.3.6, corresponding to three cavities that differ in the fraction of Aluminum and plexiglas along the path from the corner to the cavity through the exit. The theoretical prediction for an isolated bubble in perfectly conductive conditions is that the bubble volume must grow as the cub of the position coordinate and its velocity must remain constant. In isolating conditions (plexiglas) this is no longer true as the bubbles experience a decrease of temperature along their pathway. The cubic and linear fits are shown in Figs.3.7 for different cases. The agreement is satisfactory, taking into account that the conditions are not ideally conductive/isolating, and most importantly, that bubbles are not isolated. In particular, interactions between bubbles exhibit a significant number of coalescence events.

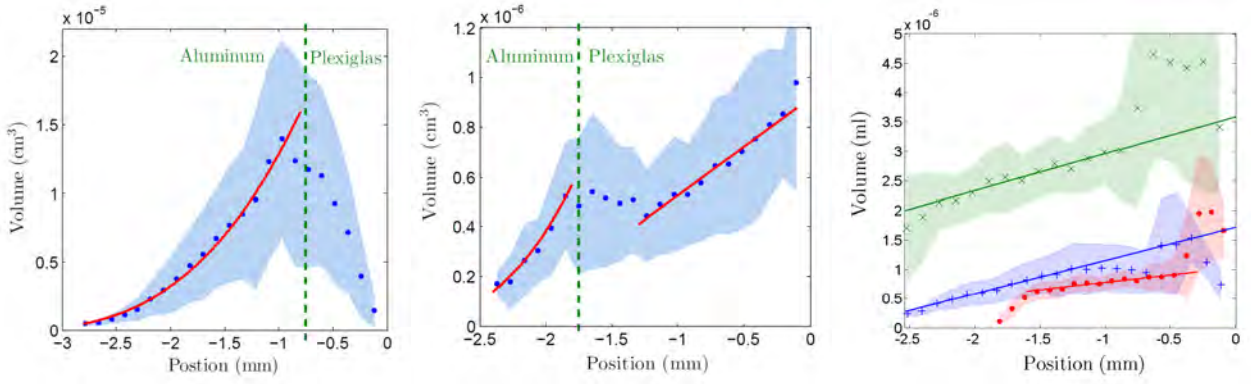

Fig.3.7 Average bubble volume along the nucleation cavity for the conductive (left) and the isolating (right) cases. The position axis has the origin at the outlet of the cavity, so that bubbles are created on the left and move to the right. At the right end, near the cavity exit, the tendency is disturbed by the effect of the crossflow. The colored shaded regions define the area covered by the standard deviation measured at each position. The dashed vertical lines mark the transition between Aluminum and plexiglass.

The test of the constant velocity prediction for the conductive case is more sensitive to the effects of bubble interactions and coalescence. In Fig.3.8 we show the measurements of mean bubble velocities along the cavity for the same three cases of Fig.3.7. The constant velocity fit is shown as a reference in the regions closer to the conductive conditions. In the plexiglass regions we fit a linear decay for the velocity for simplicity, since there is no theoretical prediction for this case, due to significant inhomogeneities of all variables.

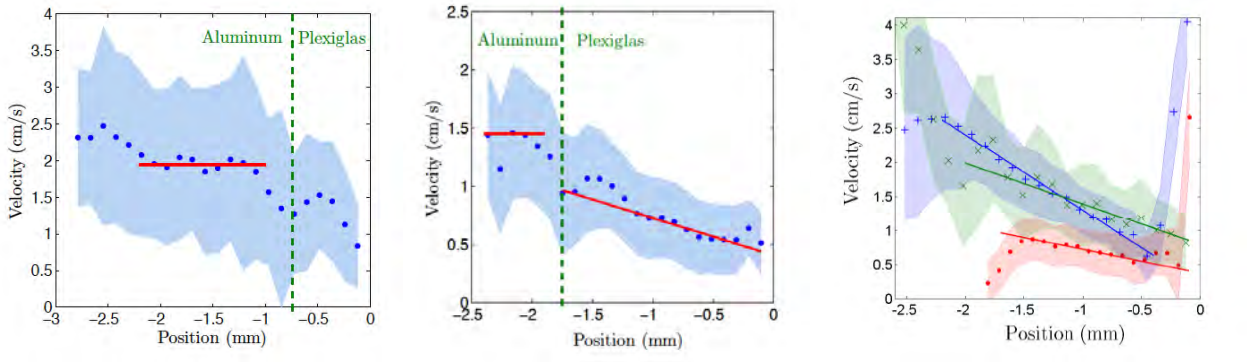

Fig.3.8 Measurements of average bubble velocities along the cavity. The position axis has the origin at the outlet of the cavity, so that bubbles are created on the left and move to the right. The colored shaded regions define the area covered by the standard deviation measured at each position. The dashed vertical lines mark the transition between Aluminum and plexiglass. Fist of constant and linear decaying velocities are shown for reference respectively in the conductive and isolating regions respectively. Strong deviations from the main tendencies are observed near the cavity outlet due to the effect of the crossflow.

Finally, as a sample of the slug flows that are generated with the improved setup, in Fig.3.9 we give three examples where both bubble size and bubble separation are varied independently. Once the spurious nucleation has been removed and the pressure transients have been virtually eliminated, the performance of the nucleation cavity is much more regular and periodic, resulting in much better slug flows. Note that this is true regardless of the conditions and dynamical regime inside the nucleation cavity, which in some cases may be quite complex due to instabilities and coalescence. Remarkably, this is not reflected in the regularity of the downstream flow.

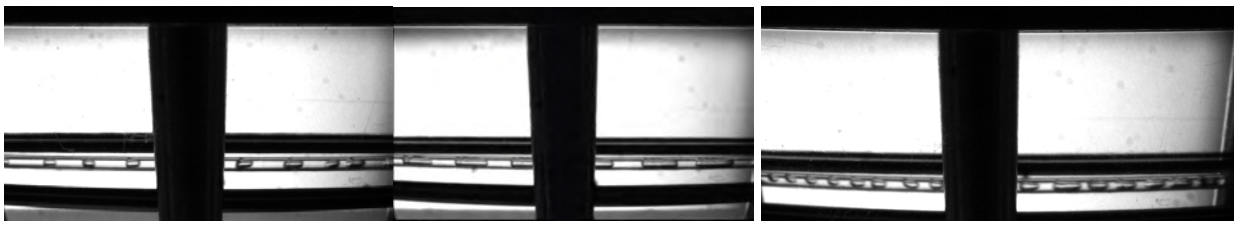

Fig.3.9 Samples of slug flows recorded by the camera located far downstream corresponding to three different experiments at 0g.

3.4 FOURTH AND FIFTH DROP TOWER CAMPAIGNS

The last two campaigns of the project were conceived with two main objectives: (i) to complete a systematic characterization and calibration of the nucleation cavity, and demonstrate the insensitivity of its performance to the gravity conditions; and (ii) to design and test a heat exchange device to illustrate and quantify the use of the slug flows created by our system.

Pressure/flow phase diagram, bubble frequency and boiling rate at the nucleation cavities

Here we present the systematic characterization of the nucleation cavity. We delimitate the boundaries between the different regimes in a phase space defined by the two main control parameters, namely pressure and crossflow. In addition we measure the frequency of bubble formation and the average bubble size at the

cavity exit. The latter allows one to quantify the residual dependence of bubble size on the different conditions and provides, together with the bubble frequency, an indirect measure of the total vapor flow produced by phase transformation at the cavity (boiling rate), which is proportional to the heat per unit time absorbed by phase change at the cavity and transmitted to the flow.

The panels of Fig.3.10 summarize the main results of the study of the nucleation cavity in a phase diagram for the operation modes of the cavity and its performance in terms of bubble frequency formation and boiling rate. The effective pressure incorporates the corrections due to pressure drop along the liquid circuit for the different liquid flow injection rates, the Venturi pressure drop at the cavity outlet, and the variations of temperature from different experiments, absorbed in the effective pressure through the Clausius-Clapeyron relation. In this way, all experiments can be compared in a single pressure/flow diagram.

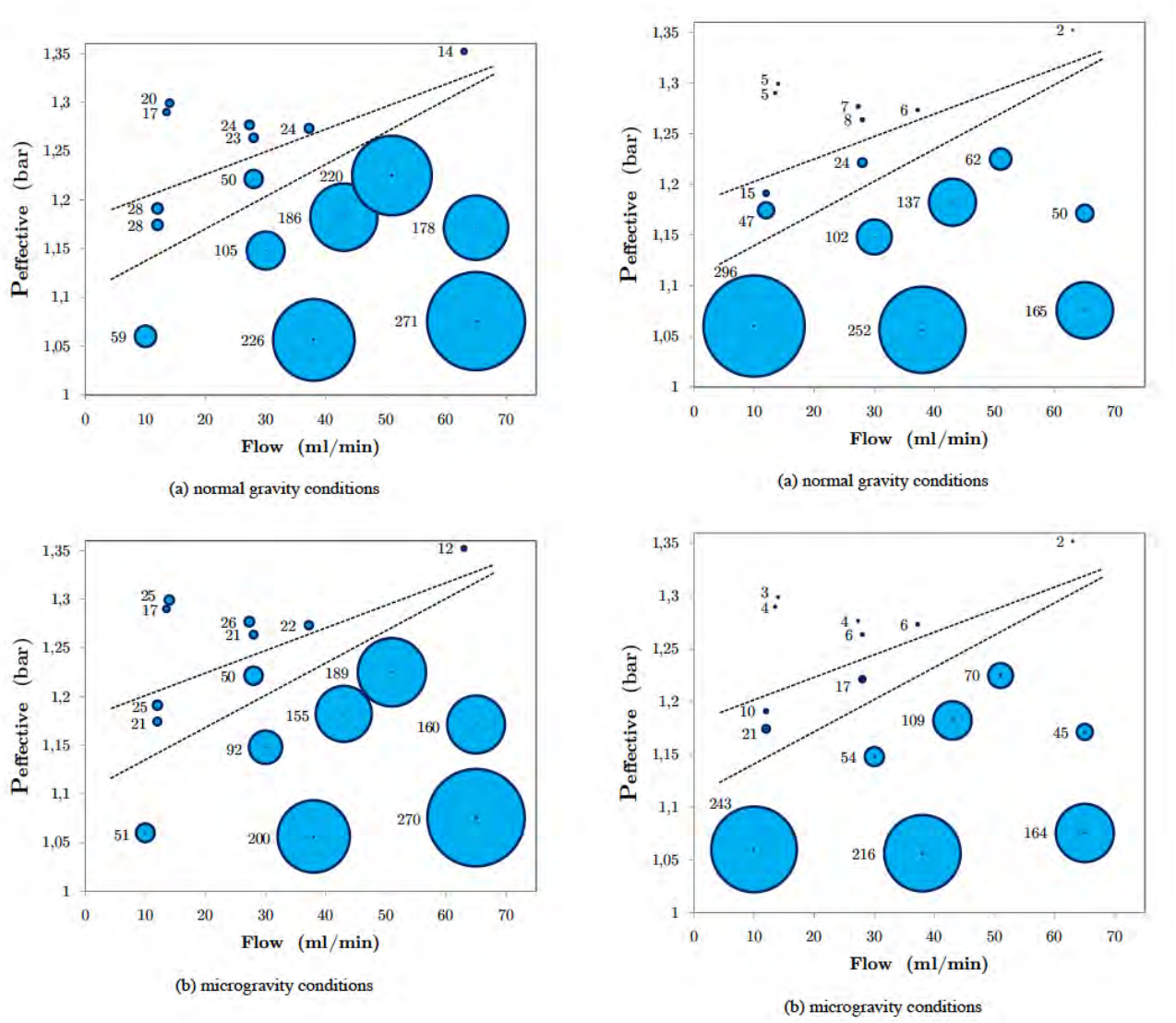

Fig.3.10 Pressure/flow phase diagram. The center point of each circle locates the conditions of crossflow volume rate injection and the effective pressure at the cavity (corrected by different effects, as explained in the text). The radius of the circle around each point is proportional to an additional degree of freedom measured at each point. For the two left panels, the radius is proportional to the average frequency of bubble formation. The number next to each circle gives the value of this frequency in number of bubbles per second. For the two right panels, the circle radius is proportional to the mass flow rate of vapor at the cavity outlet (boiling rate), in micrograms per second. The dashed lines delimitate approximately the three operating modes of the cavity, with the multiple bubble mode on top and the single bubble mode at the bottom. The intermediate mode of 1-2 bubbles is the narrow region in between. The two top panels, marked as (a), correspond to normal gravity, and those at the bottom, marked as (b), to microgravity conditions.

The main conclusions from the above panels can be summarized as follows:

(i) The performance of the cavity is essentially insensitive to gravity. The results from on-ground measurements and from drop-tower measurements have only very minor deviations that are not significant within the inherent uncertainties of the experiment. The robustness to gravity includes the location of the boundaries between the different regimes of bubble formation and both observables of bubble frequency and boiling rate.

(ii) The single-bubble regime is the one with higher boiling rate.

(iii) In the single-bubble regime, the bubble frequency formation increases significantly with the crossflow volume rate, but this is not proportional to the boiling rate, thus indicating that the bubble size at the cavity outlet has an appreciable variability, in particular for small pressures.

(iv) The boiling rate decreases systematically with pressure but it is relatively insensitive to the crosflow volume rate.

Serpentine heat exchanger device

As an illustration of a practical use of the slug flows that our system generates, we designed a metallic heat exchange device (see Fig.3.11). The metallic block contained resistors for controlled heating, and temperature probes at different locations. The slug flow at the exit of the measuring section of our system was injected as a coolant through a serpentine tube of square section.

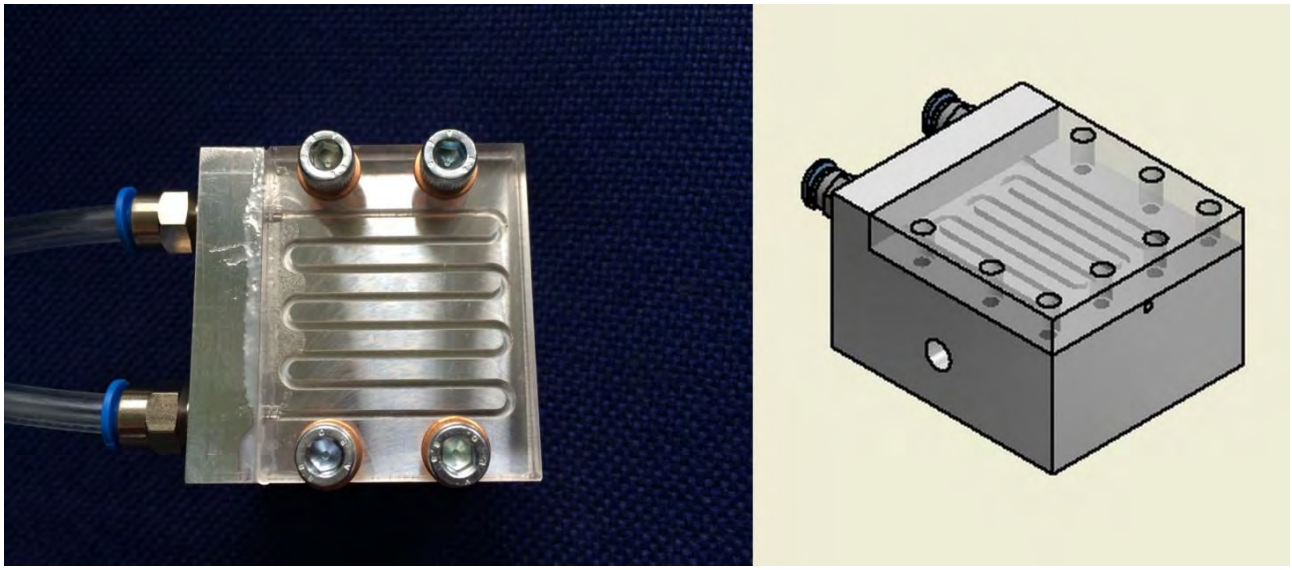

Fig.3.11 Picture and plot of the serpentine heat exchanger

Fig.3.12 shows a snapshot of the injected slug flow inside the serpentine tube. It is worth remarking the high regularity of the slug flow, both in terms of bubble size and bubble separation, which provides control of gas-liquid surface, and allows to avoid or minimize coalescence phenomena. Monitoring bubble sizes one can easily monitor the heat exchange by phase change.

Our measurements of heat exchange in this setup were for demonstrative purposes. In particular, since tested the setup both on ground and in microgravity, we assessed again the insensitivity of its behaviour to gravity. For the measurements of heat transfer, we first determined the losses to the environment from the metallic piece by measuring the steady temperature of the hot contact for different power dissipation rates imposed on the resistors. This allowed constructing the plot of heat absorbed by the injected coolant (either fully liquid or in the form of a vapor/liquid slug flow) per unit area as a function of the temperature of the hot contact, and most interestingly, as a function of the temperature difference between the hot contact and the coolant at the entry.

Fig.3.12 Snapshots of a vapor-liquid slug flows inside the serpentine heat exchanger. Left picture, example of a regular slug flow without significant heat exchange (constant bubble volume). Right picture, snapshot of an experiment in microgravity, showing the time monitoring of the movie. The growth of the bubble volume is here clearly manifest, thus visualizing the heat exchange.

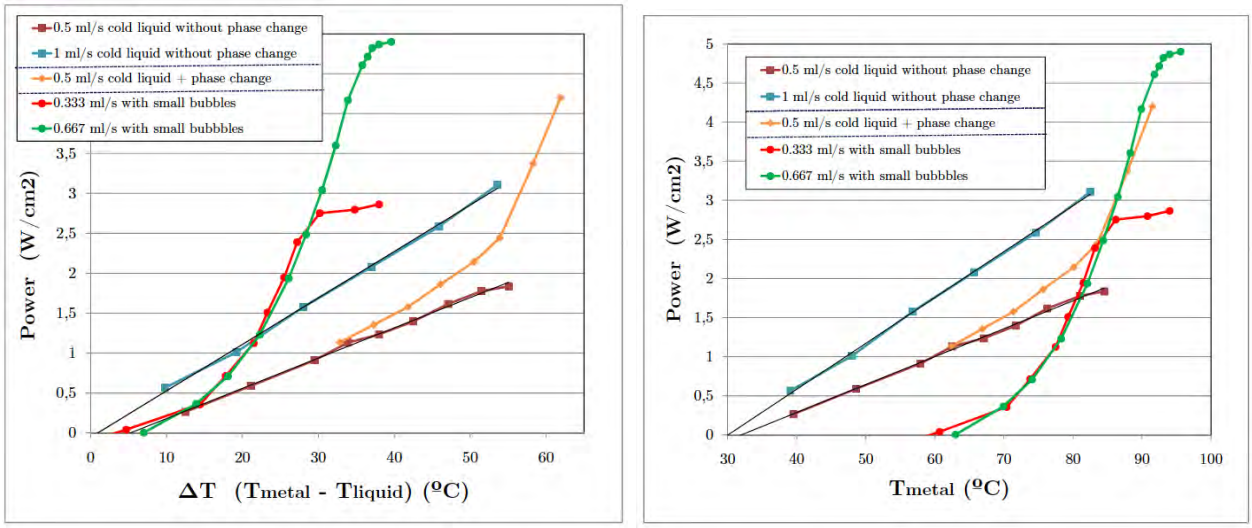

Fig.3.13 Heat exchange rate as a function of temperature. The two plots correspond to the same data. On the left panel, the power is plotted vs the temperature difference between hot metallic contact and the coolant at the entry of the device, for different injection rates of coolant, and both for full liquid or gas-liquid injection (as indicated in the inset). On the right panel the same quantity if plotted vs the actual temperature of hot contact, in the same cases.

Fig.3.13 illustrates quantitatively the efficiency of heat transfer for the case of purely liquid coolant and for a gas liquid coolant. The maximum value or heat exchange rate per unit area and per unit of degree of temperature difference achieved is around 0.15 W/cm^2 K, corresponding to the two-phase flow in the limit of practically all the liquid transformed into vapor. To increase this value, in addition to improve the geometry of the device, one should increase the coolant injection volume rate. The same figure illustrates how in the biphasic case the efficiency increases with the temperature difference, since the power per unit area grows faster than linear. For the purely liquid coolant, instead, the power per unit area grows linearly with temperature and the efficiency remains roughly constant for a given flow rate. For single phase coolant the value of the efficiency is significantly smaller than for the biphasic coolant, but it increases with the flow rate. On the contrary, for the slug-flow injection the efficiency remains independent of the flow rate as long as the liquid is not fully vaporized. When all the coolant is already vaporized, this condition fixes the

saturation of the curve at the upper bound of the efficiency for a given injection rate. This saturation value, however, can be raised by increasing the injection flow rate. It is interesting to see the crossover from the liquid coolant to the biphasic coolant in one of the cases of Fig.3.13.

3.5 ANALYTICAL AND NUMERICAL RESULTS OF FUNDAMENTAL INTEREST

Inspired from the study of the geometry of the nucleation cavity, throughout this project we have also addressed theoretically some limiting cases that shed some light in the performance of our device and at the same time provide interesting results from a fundamental point of view. The first relevant theoretical insight was to realize that a self-similar solution exists for the single-bubble problem under perfect conducting conditions (constant temperature) and in the limit of small Reynolds number (Stokes flow, inertial forces dominant over viscous forces) and small capillary number (capillary forces dominant over viscous forces). This solution implies a constant velocity of the bubble insight the cavity, and served as a reference base for the analysis of our data.

Most interestingly, we have found that a self-similar behaviour exists also in a statistical sense (in the same conditions) for multiple-bubble situations, and including coalescence events. This has been proved within a simplified model where bubbles advance at constant velocity as they grow and where coalescence events occur instantaneously (at a much faster time scale than that of the flow, as consequence of the small capillary number limit). An exact analytical result has been obtained within this model that proves that the density of bubbles ρ is statistically self-similar and scales with a universal exponent with the distance x along an infinite cavity, taking the form

$$\rho = \frac{A}{x}, \quad A = \frac{1}{4}\left[1+\cot\left(\frac{\theta}{2}\right)\right]$$

where θ is the angle of the nucleation cavity (see Fig.3.14). This result is exact for the case of periodic bubble nucleation but has been extended to more general cases with stochastic nucleation and other more general cases that relax some of the assumptions of the model. The numerical simulations of these more general cases, however, shows also excellent scaling properties as shown in Fig.14, and indicates that the scaling exponent is indeed universal.

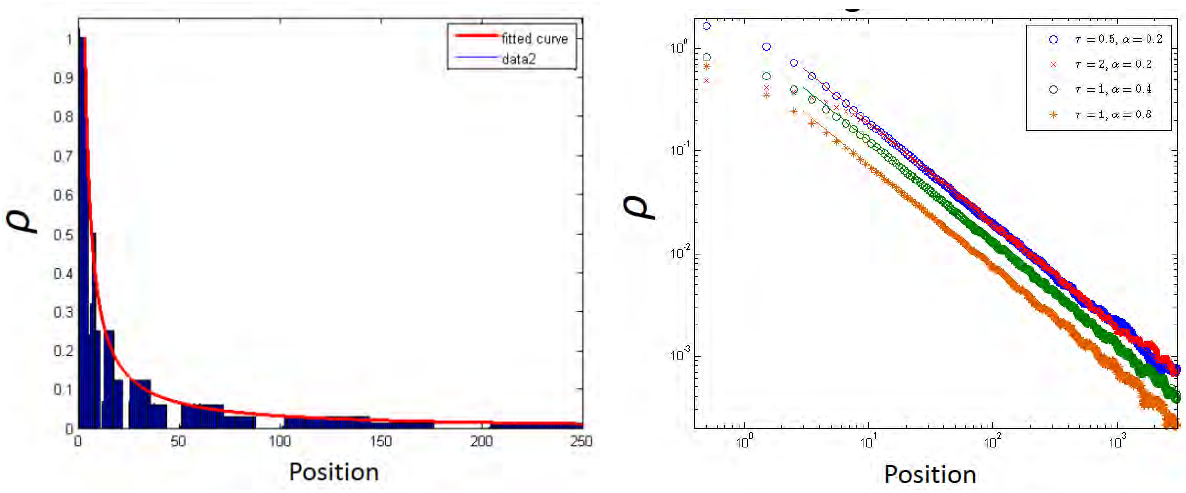

Fig.3.14 Analytical and numerical results for the idealized model of the conducting nucleation cavity. On the left, exact result for the bubble density as a function of distance from the cavity corner. The red curve is the exact result shown in the text. On the right, numerical simulation of the model for the more realistic cases with random nucleation of bubbles with a frequency of bubble formation given by τ^{-1} and for different values of α, a parameter that controls the growth rate (i.e. boiling rate), showing excellent scaling with the universal exponent.

The universal character of the exponent, and the fact of having identified an idealized model of nucleation that can be solved exactly give these results a very interesting fundamental dimension.

4 CONCLUSION

In this project we have designed, tested and optimized a prototype system for capillary boiling that produces in a robust, controlled and gravity-insensitive way trains of bubbles of regular spacing and bubble size of the order of the capillary diameter, as the bubbles are injected in a liquid crossflow at the outlet of the nucleation cavity. The performance of the system has been systematically characterized for a broad range of pressure and crossflow conditions, identifying different modes of operation and measuring the bubble frequency production and the corresponding boiling rate. The capillary slug flows thus created can be used for applications in either the study of heat transfer or in possible technological applications. The key advantage of the outcome of our method is that it supplies bubbles of controlled size at a regular rate, thus providing control of surface/volume ratio (fixed by the bubble size), and relative control of coalescence phenomena (crucially affected by the bubble separation in the bubble trains). Given the inherently unstable and delicate nature of the phenomenon of bubble nucleation of an overheated liquid (a metastable state), and the general difficulty to control the heat transfer rate, we believe that the degree of success in achieving our goal is remarkable. Furthermore, in our study we also pursued some fundamental questions raised by the proposed setup and obtained interesting theoretical insights and exact analytical results that are relevant in the study of scaling and universality in the kinetics of phase transitions.

The results on the performance of the nucleation cavity are currently being collected in a manuscript that we intend to submit in the near future to the American Institute of Aeronautical and Astronautical Journal under the title *Capillary boiling through controlled nucleation in microgravity* by P. Bitlloch, X. Ruiz, L. Ramírez-Piscina and J. Casademunt. We have finally discarded filing a patent on our device and process. On the other hand, the theoretical studies of an idealized nucleation cavity under perfectly conducting walls are planned to be submitted to a high impact, general physics journal like Physical Review Letters, by the same authors and under the tentative title of *Scaling and universality of capillary boiling in a tetrahedral geometry. An exactly solvable model.*

6 APPENDICES

APPENDIX A: DESCRIPTION OF THE EXPERIMENTAL APPARATUS

Table of elements and specific models used in the experimental setup.

	Name	**Model**
1	Liquid Pump	Pump: Micropump DG-D42.H2S2P5.M.B Pump head: Micropump GA-X21.P9FS.M
2	Liquid Filter	Filter paper element – MannHummel WK 31/2
3	Liquid flow-meter	Kobold flow meter PEL-L000SPFFY
4	Manual valve	Festo QH-QS-6
5	Manual throttle	Festo GRO-QS-6
6	Small receptacle	Plexiglass, ~ 15 ml
7	Medium bath	Stainless steel tube: 3mm inner diameter, 4mm outer diameter, 6 loops of 10cm diameter. Total length=2181mm
8	Hot bath	Stainless steel tube: 1.76mm inner diameter, 3.18mm outer diameter, 8 loops of 10cm diameter. Total length=2808mm
9	Measuring section	Plexyglass. More details below
10	Cold bath	Same as num 7 - Medium Bath
11	Pressure limited valve	Swagelok SS-RL3S6MM
12	Security reservoir	Plastic - ~ 500 ml
13	Phase separator	Plexiglass receptacle of ~ 300 ml with a metallic mesh (with square holes of 0.2mm size) at the exit tube
14	Liquid reservoir with air pressure	Modification of Festo DNG-32-200-PPV-A with transparent receptacle (of 31.8mm inner diameter) and without piston.
15	Manometer	15a) Festo SDE5-D2Z-NF-Q6-V-K (gas only) 15b) Burster Typ 8227
16	Pressure regulator valve	Festo VPPM-6L-L-1-G18-0L2H-A4N
17	Air filter	Festo LF-D-5M-MINI XN43
18	Pressured air reservoir	Festo CRVZS-0.75 (Volume=750ml)
	Cameras	2 Camera head: Photron MH4-10k s/n Camera recorder: Photron Fastcam MC2
	Tubing	4mm Gas tubes: Festo PUN-H-6x1 3mm liquid tubes: Swagelok ASTM D3307 Type II
	Batteries	4 batteries of 12V – CTM CTC26-12

Main changes between the campaigns of October 2013 and January 2014 (see Figs. A.1 and A.2):

- Pressure sensor 15b for control of the transition 1g to 0g
- Cold bath 10 located at same height than test section 9, to reduce transient effects and back flow due to gas accumulation after the test section during preparation at 1g.
- Bypass junction after 15b to avoid gas accumulation after that point, with an additional flow of cold liquid

- Tube/Valve system improved for optimization of the preparation of the experiment, allowing for more efficient boiling of all the fluid in the system to eliminate any trace of air in solution.

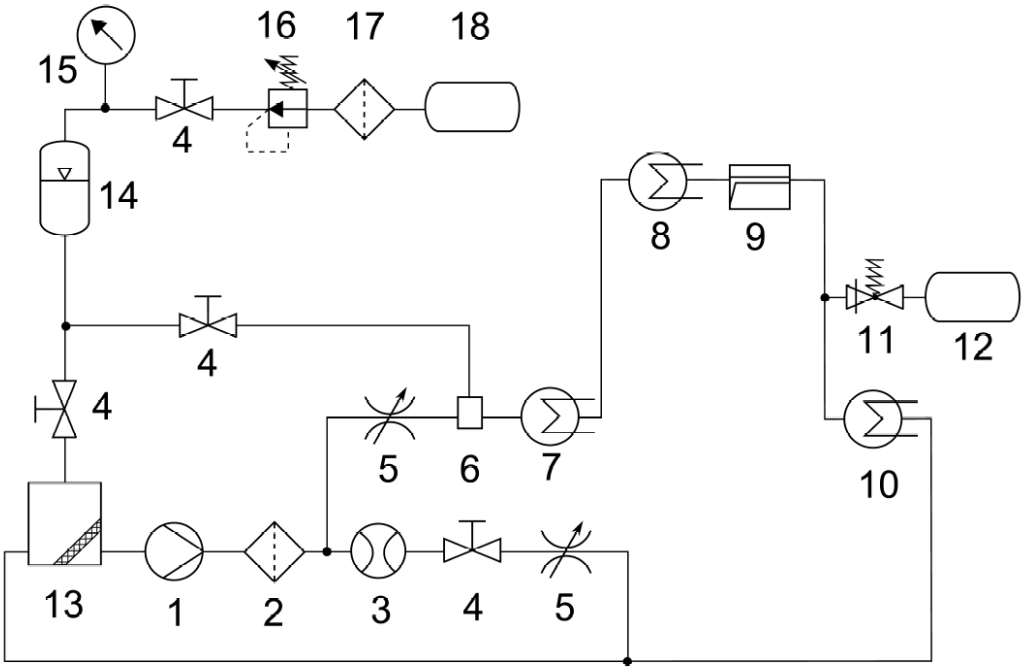

Fig.A.1 Scheme of the experimental design used in the campaign of October 2013.

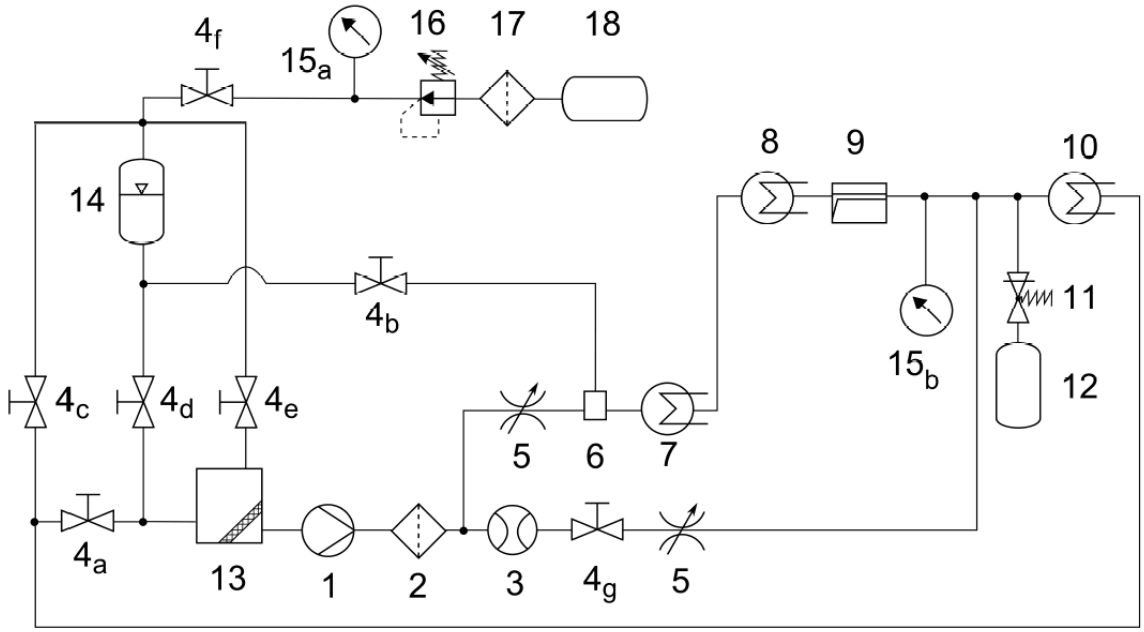

Fig.A.2 Scheme of the experimental design used from the campaign of January 2014 on.

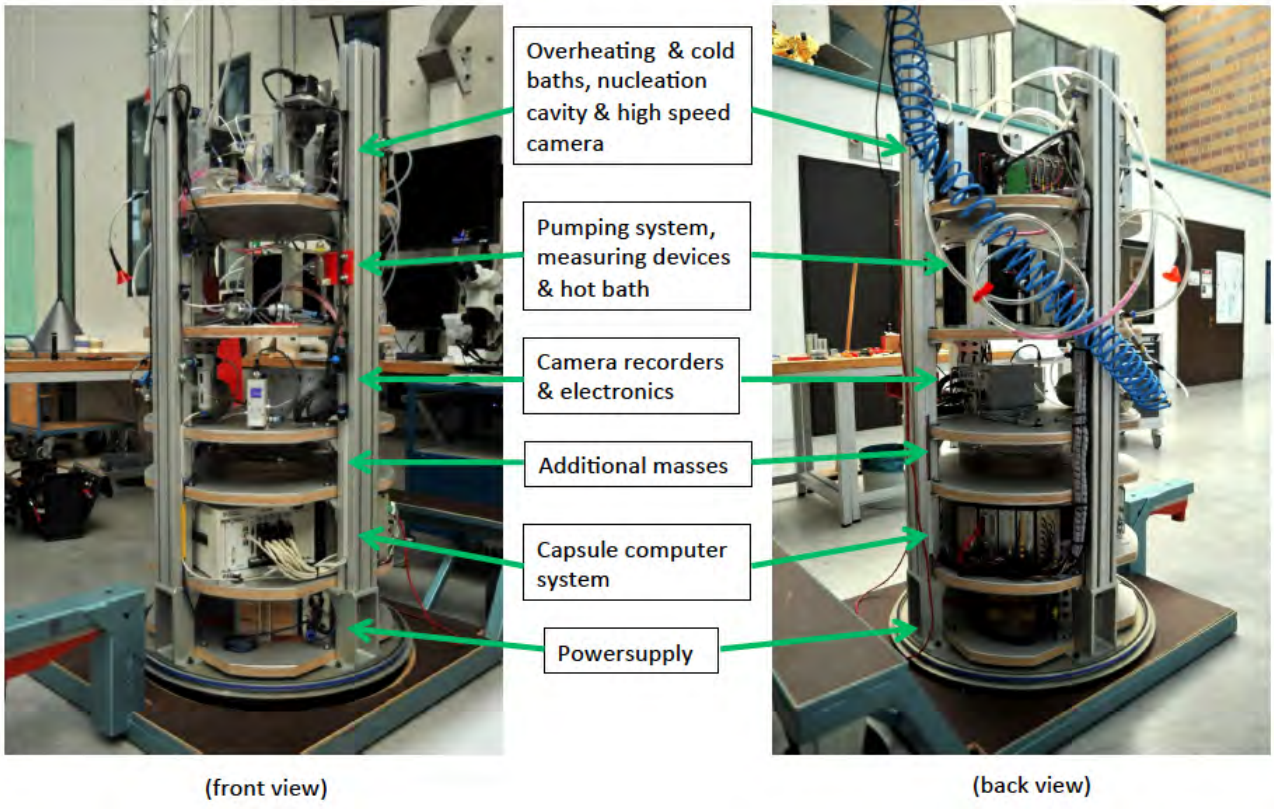

Fig.A.3 Front and rear views of the experimental setup assembled in the capsule.

Fig.A.4 View of the drop capsule inside the ZARM Drop Tower, and aerial view of the tower.

APPENDIX B: DESIGN OF THE NUCLEATION CAVITY

The V-shaped nucleation cavity was originally constructed as a 'sandwhich' of two equal plexiglass pieces as described in Fig.B.1

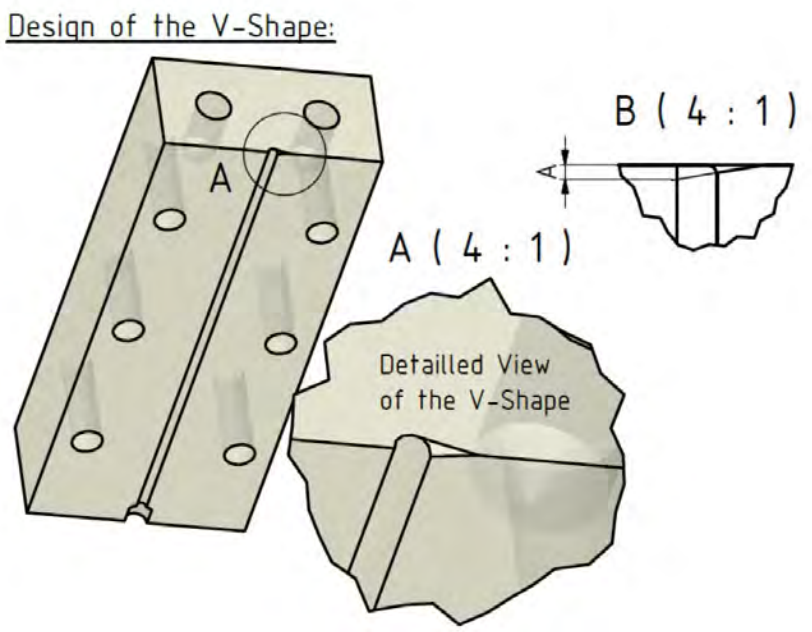

Fig.B.1 Basic cut of each of the sandwich pieces for the V-shaped nucleation cavity.

This was done for facility of construction. However, the existence of a juncture line is a potential source of spurious nucleation. A cut of the plexiglass in a single piece that avoids the contact line is only possible with curved boundaries, giving rise to a U-shaped cavity. The advantages of this design are (i) elimination of the juncture line; and (ii) better optical access. However, there are some disadvantages: (i) the cut is usually more irregular; (ii) the length of the drilled capillary tube is limited, and several consecutive pieces must be assembled; (iii) the theoretical analysis in terms of self-similar bubble solutions is less accurate. In any case, the main objective of avoiding spurious nucleation was only partially achieved and the U-shaped design was abandoned when a better solution was found.

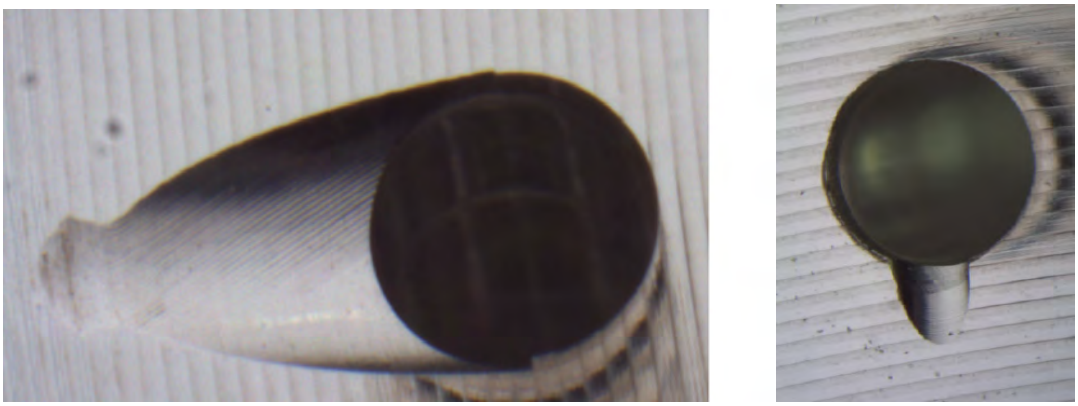

Fig.B.2 Images on the microscope of the U-shaped cavity.

The design that is currently being used consists of only one of the pieces described in Fig.B.1, assembled to an uncut block of plexiglass, in such a way that the nucleation cavity is half of the originally tested. This design is the one that allows a horizontal orientation of the cavity so that the differences between the 1g and the 0g cases are minimized.

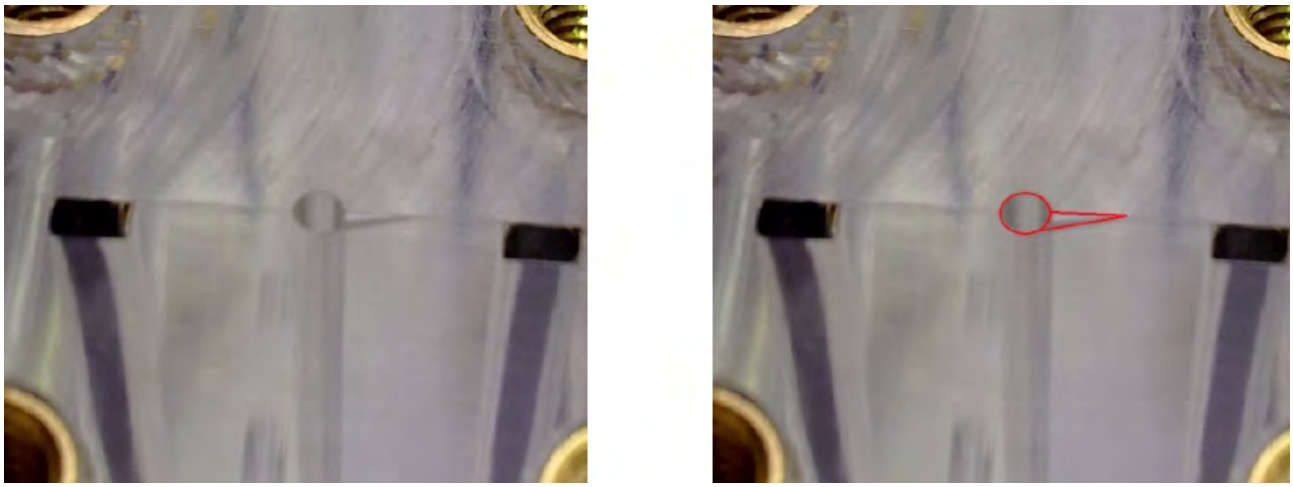

Fig.B.3 Direct and highlighted views of half V-shaped cavity.

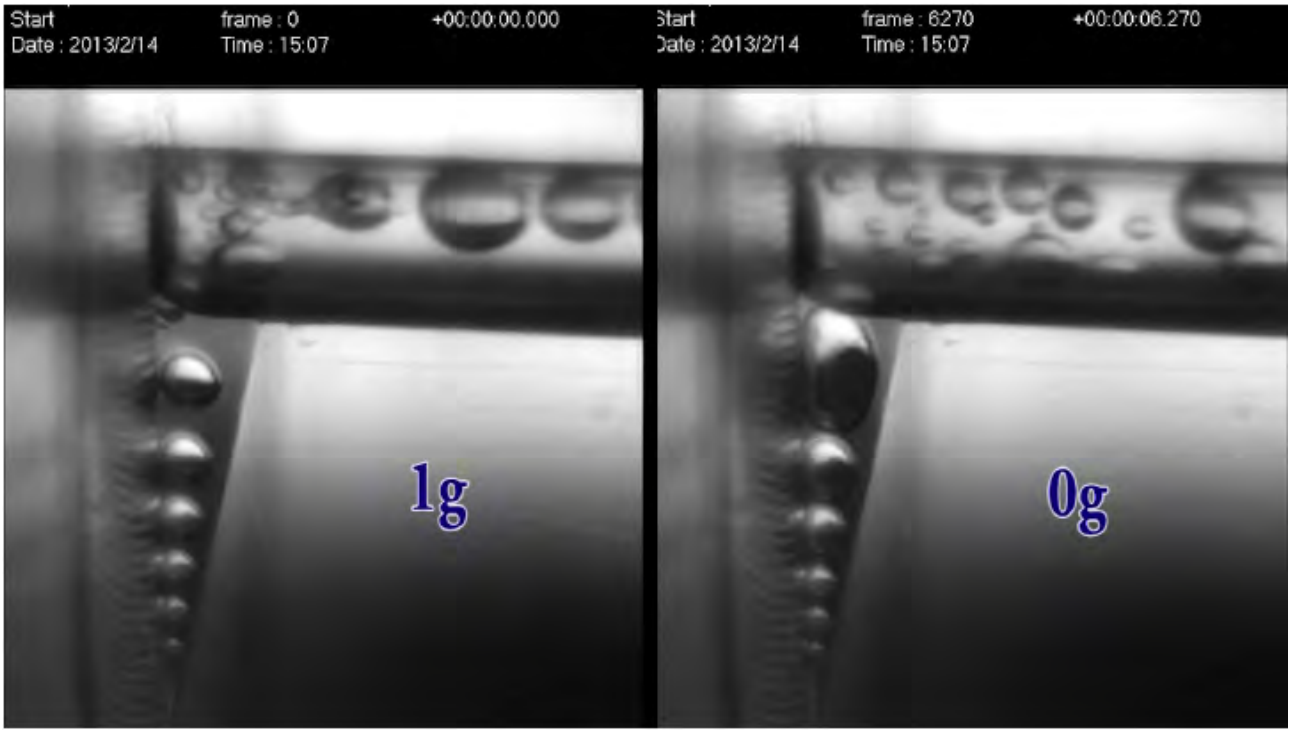

Fig.B.4 Examples of spurious nucleation at its worst, for both 1g and 0g. Many of the bubbles in the capillary crossflow do not originate at the V-shaped cavity, but at the juncture of the two plexiglass pieces that close the capillary tube, right on top of the pictures.

APPENDIX C. DESIGN OF THE ALUMINUM HEATCARTRIDGE.

The part that connects the exit of the hot bath to the measuring section must contain an additional metallic cartridge heater to overheat the liquid right before the nucleation cavity. The original design consisted of two assembled pieces of Aluminum that covered the capillary tube as shown in Fig.C.1(a)

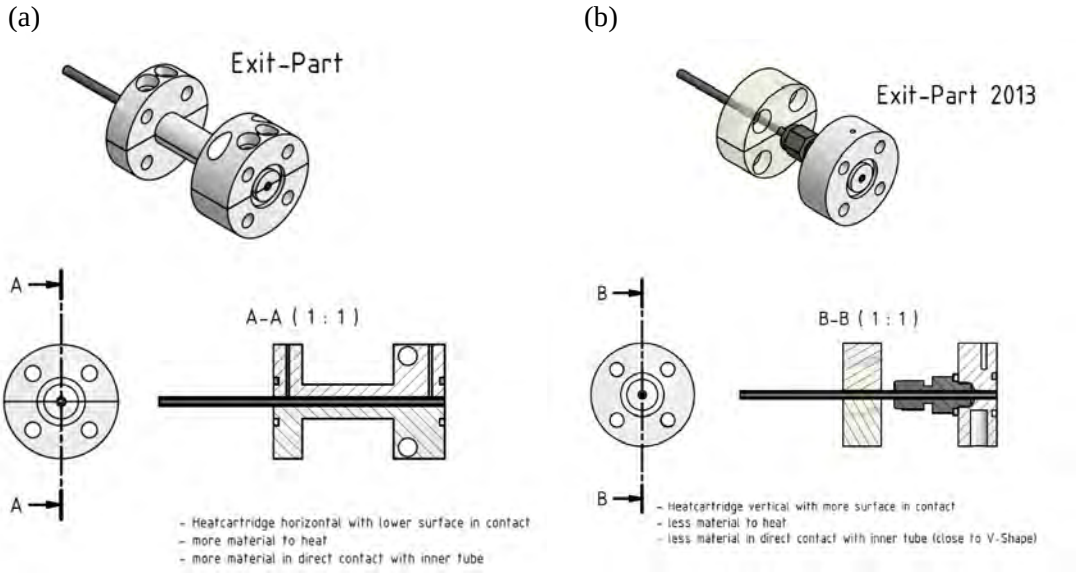

Fig.C.1 Aluminum heatcartridge covering the steel tube coming from the hot bath, in the original design with two Al pieces (a); and with a single Al piece (b).

As mentioned before, the existence of juncture lines is a potential danger for spurious nucleation. As a second attempt to minimize this undesired effect (after the U-shaped cavity discussed in Appendix B), we tried a design with a single Al piece. This turned out not to work satisfactorily because the length of the contact between the Al piece and the steel tube (see Fig.C.2(b) lower panel) was much smaller than in the previous design (Fig.C.1(a) lower panel). The Al had then to be heated at higher temperatures, and the strong temperature gradients worked against the reduction of the spurious nucleation, even when the surfaces were polished with extreme care.

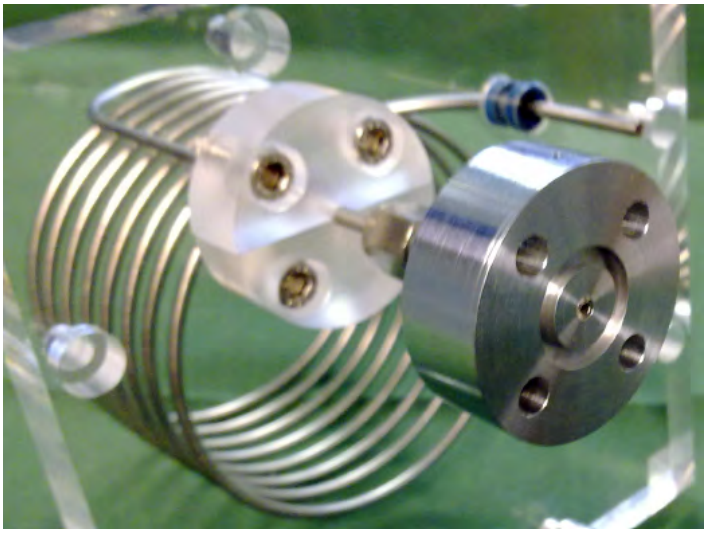

Fig.C.2 View of the single-piece heatcartridge.

The solution of the spurious nucleation problem was satisfactorily achieved yet with a new design, after noticing that nucleation occurred mostly at the contacts between metal and plexiglass. Hence the crucial point is that this contact (outside the actual nucleation cavity), must occur as far as possible upstream before that cavity, that is, in a realtively colder region. This is achieved with the new design shown in Fig.C.3, where a wide piece of plexiglass lies in between the two metallic sections. The tube inside is of plexiglass and the contact of this with the metal occurs far to the left in Fig.C.3. In addition, the metallic heater in the middle is significantly wide and can overheat the liquid in the absence of any junctures.

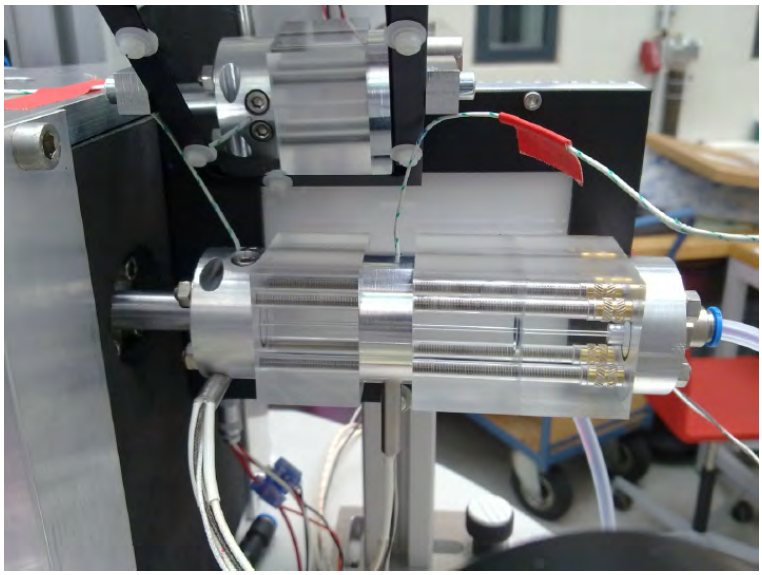

Fig.C.3 Final setup at the exit of the hot bath, showing a wide piece of plexiglass before the metallic heater.

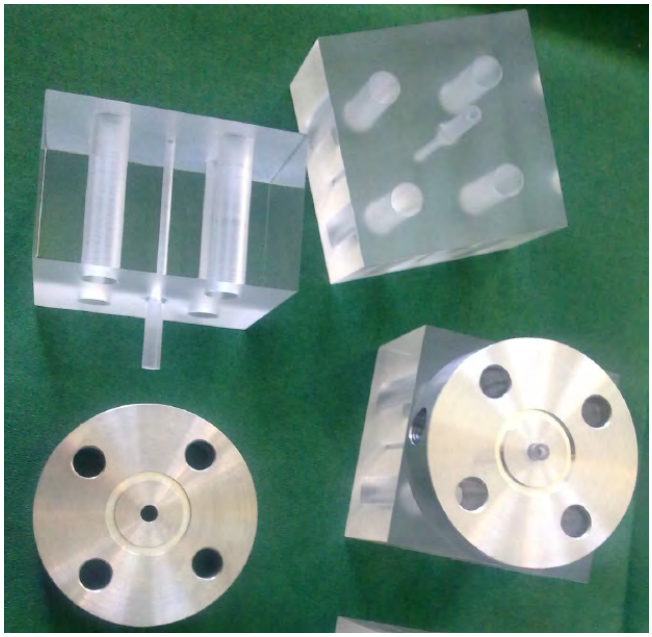

Fig.C.4 Final design of the critical pieces between the hot bath and the measuring section: two views of the same plexiglass piece, and two views of the metallic piece, unassembled and assembled to the plexiglass one.

APPENDIX D. EXPLORATION OF NUCLEATION BY VENTURI EFFECT

In paraller to these developments, we tentatively explored a drastically different design as a possible alternative in case that the spurious nucleation could not be fully avoided. The idea was to trigger the nucleation with the sudden and local pressure drop due to a narrowing of the tube, by Venturi effect. We estimated that the section of the capillary had to be reduced from a diameter of 1.5 mm down to one of 0.4 mm, so that a high pressure would prevent nucleation at any other part of the liquid line except at the nucleation point. The uncontroled part of the method was whether the nucleated bubbles would breakup into small ones due to the high velocities achieved at the narrowing of the tube, and consequently how regular would eventually be a slug flow generated by this procedure. It turned out that the method worked as a bubble generator but it was very unstable and sensitive to parameters. With small changes of parameters it would change between a mode of operation that created large numbers of very small and irregular bubbles, to a mode where a single very elongated bubble was formed and breaked up irregularly into smaller bubbles at a distant point. We concluded that the control of this alternative method seemed more challenging and we abandoned this idea when we found an appropriate solution to the spurious nucelation problem, as discussed in Appendix C.

(a) (b)

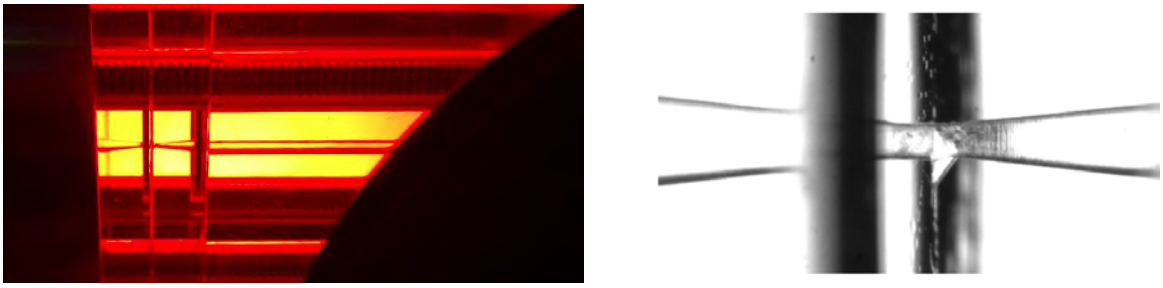

Fig.D.1 (a) View of the measuring section including the Venturi (narrow) junction of the capillary tube; (b) Detail of the Venturi junction, where a small V-shaped cavity was also added to favor nucleation.

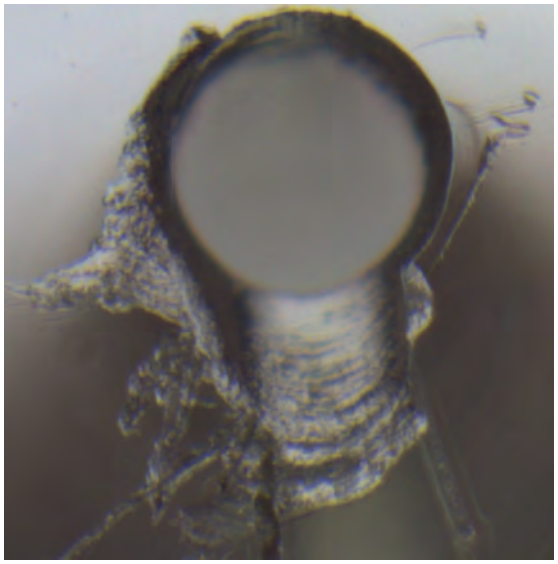

Fig.D.2 View on the microscope of a U-shaped nucleation cavity at the interior of the Venturi tube.

APPENDIX E. IMPROVED SETUP FOR OPTIMAL PRESSURE CONTROL

A significant improvement of the setup has been achieved by modifications of the setup at the outlet of the measuring section. It is particularly crucial the bypass between 15b and 11 (see Fig.A.2). This introduces cold liquid at an area where it is crucial to prevent the accumulation of vapor during the 1g phase of the experiment. The liquid drags and/or condenses residual bubbles that may be trapped in that area. The cold bath has also been relocated at the same height as the measuring section. This is important to avoid pressure transients due to the sudden change of hydrostatic pressure in the transition to 0g. The manometer 15b has also become important to monitor the variation the nominal pressure at 1g and at 0g. We have virtually eliminated the transients observed in the first campaign are have now virtually the same pressure before and after the drop release.

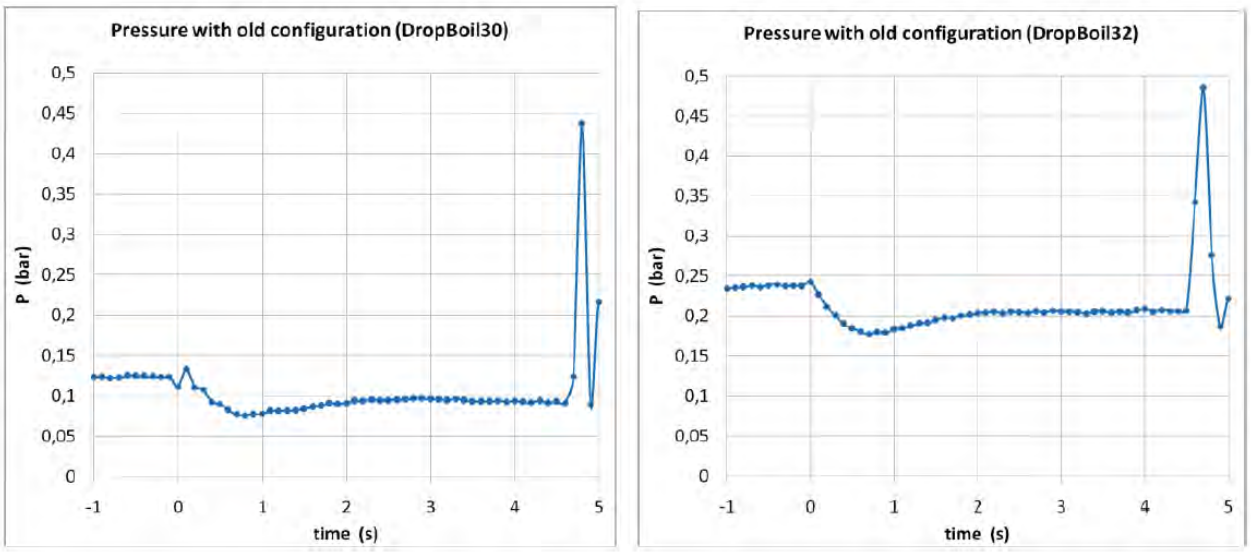

Fig.E.1 Two exemples of the pressure evolution in the original setup. Note the transient after t=0 (transition to 0g) and the different limiting value for 0g and 1g (the peak at t=4.7 corresponds to the sudden slow down at the end of the drop)

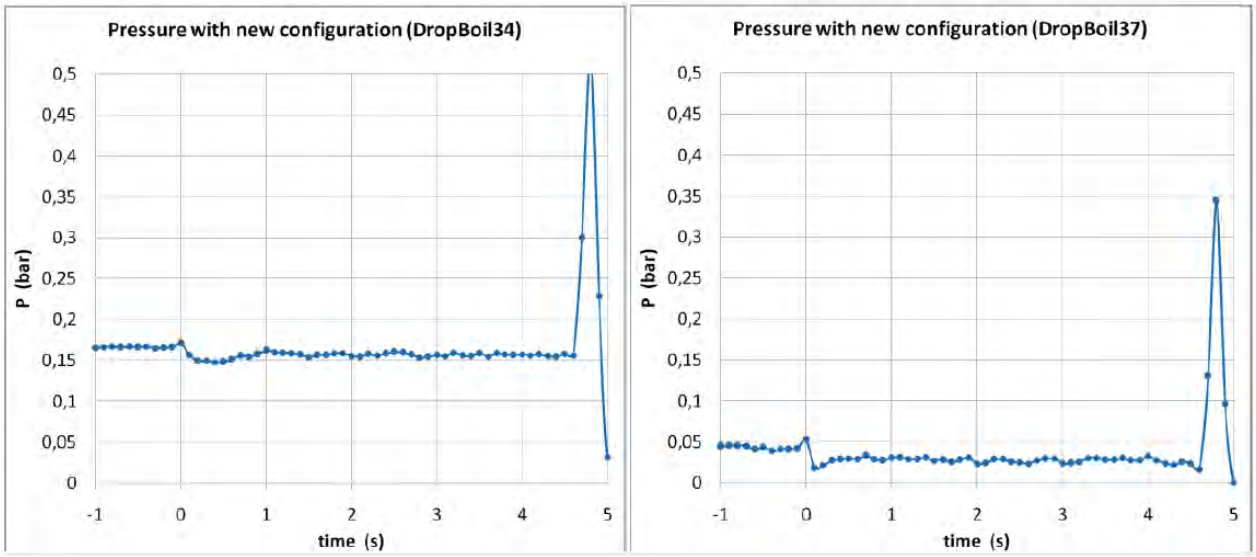

Fig.E.2 Two exemples of the pressure evolution in the modified setup. Note that the transient after t=0 is virtually eliminated and that the asymptotic value at 0g is very close to the value at 1g (before t=0).

APPENDIX F. PHYSICAL PROPERTIES THE FLUID EMPLOYED (FC-72)

The most relevant physical properties and technical specifications of the fluid employed in our experiments are summarized in the document provided by the supplier, which we partially reproduce below.

3M

Fluorinert™ Electronic Liquid FC-72

Product Information

Introduction

3M™ Fluorinert™ Electronic Liquid FC-72 is a clear, colorless, fully-fluorinated liquid. Like other Fluorinert electronic liquids, Fluorinert liquid FC-72 is thermally and chemically stable, compatible with sensitive materials, nonflammable, practically non-toxic and leaves essentially no residue upon evaporation. This unique combination of properties makes Fluorinert liquid FC-72 ideal for many electronics applications, including quality and reliability testing.

Fluorinert liquid FC-72 conforms to Military Specification 883 as a detector fluid in a vacuum/pressure vessel used in gross leak testing. Its inert nature makes FC-72 liquid a useful reaction medium.

Physical Properties

Not for specification purposes

All values determined at 25°C unless otherwise specified

Properties	FC-72
Appearance	Clear, colorless
Average Molecular Weight	338
Boiling Point (1 atm)	56°C
Pour Point	-90°C
Estimated Critical Temperature	449 K
Estimated Critical Pressure	1.83 x 10^6 pascals
Vapor Pressure	30.9 x 10^3 pascals
Latent Heat of Vaporization (at normal boiling point)	88 J/g
Liquid Density	1680 kg/m^3
Kinematic Viscosity	0.38 centistokes
Absolute Viscosity	0.64 centipoise
Liquid Specific Heat	1100 J kg^{-1} C^{-1}
Liquid Thermal Conductivity	0.057 W m^{-1} °C^{-1}
Coefficient of Expansion	0.00156 °C^{-1}
Surface Tension	10 dynes/cm
Refractive Index	1.251
Water Solubility	10 ppmw
Solubility in Water	<5 ppmw
Ozone Depletion Potential	0

3M™ Fluorinert™ Electronic Liquid FC-72 Electrical Properties

Properties	FC-72
Dielectric Strength	38 kV, 0.1" gap
Dielectric Constant	1.75
Electrical Resistivity	1.0×10^{15} ohm cm

Heat Transfer Properties

The following formulas can be used to calculate the specific heat, thermal conductivity and density of 3M™ Fluorinert™ Electronic Liquid FC-72 at various temperatures.

Specific Heat ($J\ kg^{-1}\ C^{-1}$) = 1014 + 1.554 (T, °C)

Thermal Conductivity ($W\ m^{-1}\ °C^{-1}$) = 0.060 – 0.00011 (T, °C)

Density (kg/m^3) = 1740 – 2.61 (T, °C)

Log_{10}(Vapor Pressure (pascals)) = 9.729 – (1562/(T, K))

The following graph can be used to determine the viscosity of Fluorinert liquid FC-72 over the indicated temperature range.